JGR Space Physics

RESEARCH ARTICLE
10.1029/2019JA027001

Key Points:
- Presence of 'cusp' signatures in the ionograms during Nepal earthquake
- Signatures of possible acoustic and atmospheric gravity waves in the ionosonde observations during Nepal earthquake
- GPS TEC observations shows the propagation of Rayleigh wave induced acoustic waves in the ionosphere

Supporting Information:
- Supporting Information S1

Correspondence to:
S. Sripathi,
ssripathi.iig@gmail.com

Citation:
Sripathi, S., Singh, R., Tiwari, P., & Kumar, M. R. (2020). On the co-seismic ionospheric disturbances (CIDs) in the rapid run ionosonde observations over Allahabad following M_w 7.8 Nepal Earthquake on April 25, 2015. *Journal of Geophysical Research: Space Physics*, *125*, e2019JA027001. https://doi.org/10.1029/2019JA027001

Received 6 JUN 2019
Accepted 17 DEC 2019
Accepted article online 3 JAN 2020

On the Co-Seismic Ionospheric Disturbances (CIDs) in the Rapid Run Ionosonde Observations Over Allahabad Following M_w 7.8 Nepal Earthquake on April 25, 2015

S. Sripathi[1,4], Ram Singh[1], Prabhakar Tiwari[2], and M. Ravi Kumar[3]

[1]Indian Institute of Geomagnetism, Navi Mumbai, India, [2]Dr. K. S. Krishnan Geomagnetic Research Laboratory, Indian Institute of Geomagnetism, Allahabad, India, [3]National Geophysical Research Institute, Hyderabad-500007, [4]On deputation to ICTP, Trieste, Italy

Abstract We present high-resolution ionosonde observations at Allahabad (25.43°N, 81.84°E) near anomaly crest location in India along with GPS TEC to investigate the possible signatures of co-seismic disturbances (CIDs) in the ionosphere during M_w7.8 Nepal Earthquake that occurred at 06:11:26 UT on 25 April 2015. The epicenter of the earthquake (28.147°N, 84.708°E) was located at ~77 km north-west of Kathmandu with a shallow depth of 15 km. The mechanical shock disturbances produce Rayleigh waves and Rayleigh wave induced acoustic gravity waves (AGWs) during earthquake which propagate into the ionosphere and produced plasma density fluctuations due to collisions. The manifestation of these waves produces 'wiggles' or 'cusps' in the ionograms known as Multiple-Cusp Signatures (MCS). The detection of multiple cusps in the ionograms at Allahabad indicates the altitude structure of Rayleigh wave and it's induced AGWs. To confirm co-seismic signatures in ionosonde further, we scaled the ionograms at iso-density and iso-heights along with foF2 (MHz) and h'F (km). The periodogram and wavelet analysis suggest the presence of acoustic gravity waves and gravity waves with frequencies in the range of 0.7-1.5 mHz over the altitude range of 180-250 km. The foF2 variations show wave like oscillations having frequency of 0.5 mHz after the onset of earthquake. The GPS TEC also show signatures of co-seismic perturbations having frequencies in the range of 2-4 mHz and are propagated to southward with a speed of 0.5-1.0 km/s. These results suggest that there exists a good coupling between seismic activity and ionized density perturbations after Nepal earthquake.

1. Introduction

Earth's ionosphere is a transition region between neutral dominated lower atmosphere at the below and plasma dominated region at the topside of the atmosphere. Accordingly, the ionospheric electron density is affected by forcing from below such as atmospheric waves and tides and forcing from above such as solar flux and geomagnetic storms (e.g., Forbes et al., 2000; Rishbeth & Mendillo, 2001). Several studies have been made in the past to understand the forcing of waves from lower atmosphere as well as forcing from the solar sources on the ionosphere (e.g., Forbes et al., 2000; Rishbeth & Mendillo, 2001; Chau et al., 2009, 2010). In the recent past, it is increasingly evident that ionospheric density is also affected by natural hazards such as cyclones, earthquakes and tsunamis (e.g., Afraimovich et al., 2001; Dasgupta et al., 2006; Astafyeva et al., 2009; Occhipinti et al., 2010; Maruyama et al., 2011; Rolland et al., 2011; Reddy & Seemala, 2015). It is known that these natural hazards cause major threat to the human lives and several people are affected across the globe due to these events. The deadliest events among them cause severe human loss and damage to property. While severe weather events are monitored and forecasted by weather agencies using meteorological observations such as balloons, weather radars and satellite images along with weather prediction models, earthquakes are detected mainly by seismometers. The seismometer can monitor the movement of earth using seismic waves such as Primary waves (P-wave), Secondary or Shear waves (S-wave) and Rayleigh surface waves (e.g., Komjathy et al., 2016). The Energy released during an earthquake travels in the form of seismic waves around the Earth. It is believed that S-waves and surface waves are more dangerous than P-waves. They travel differently through the different parts of the Earth. Since P-wave reaches the surface faster than S-wave and Rayleigh waves, it is possible to know the occurrence of earthquake only few

seconds prior. But the lead time is very short to be used for early warning systems. Similarly, tidal gauges are used to detect tsunamis but they also can't help if the direction of tsunami wave changes suddenly to opposite direction to the location of tidal gauge. Accordingly, several studies have been carried out to understand these seismic events to identify their arrival ahead of time so that it can be used for alerts. Past studies have shown that ionospheric disturbances due to earthquakes can be observed using HF Doppler sounding technique (e.g., Davies and Baker, 1965; Yuen et al., 1969). Liu et al. (2006) have investigated the Rayleigh surface wave induced atmospheric gravity waves due to Sumatra earthquake on 26 December 2004 using Doppler sounding system. The ionospheric disturbances due to 2011 Tohuku earthquake, 2004 Giant Andaman earthquake and Nepal earthquake have been investigated using low power Doppler sounding system (Artru et al., 2004; Chum et al., 2012, 2016). Using this system, the results suggest that the infrasound waves which are detected in the ionosphere are consistent with their travel times when one considers the propagation time delays into account. Najita and Yuen (1979) were the first to suggest that HF Doppler is very sensitive tool to detect the infrasound waves in the ionosphere when Earthquake induced Rayleigh waves excite shock acoustic waves at the surface and propagated through the atmosphere. Using dispersion relation, they suggested that it is possible to derive dispersion curves for Rayleigh waves. The application of these curves is that source location can be identified at the surface.

Earthquakes are mostly produced at the subduction zones where one plate colloids with other. It is believed that mechanical signatures such as acoustic and gravity waves, chemical signatures such as radon gas emission and electromagnetic signatures such as ELF/VLF wave emissions near the earthquake preparatory zones are being used to study the pre or co-seismic signatures in the ionosphere (e.g., Pulinets & Boyarchuk, 2004; Heki, 2011; Maurya et al., 2016). The ground motion near the epicenter causes air to oscillate producing wave perturbation. Due to decrease of mass density with altitude, the amplitude of these waves keeps increasing for the same energy. The neutral atmospheric waves which are propagated to ionospheric altitudes interact with ionized medium through collisions which produces density oscillations in the medium. The ionospheric disturbance which are excited by Rayleigh surface waves propagate with velocity of 3.3 km/s. These waves become more pronounced when they propagate far distances. It is believed that ionospheric density can be perturbed by three processes during earthquakes namely (a) acoustic gravity wave modulating the E region electric fields which in turn modify the F region density through E region dynamo, (b) direct penetration of acoustic waves into the F region to produce density perturbation and (c) density modulations observed at E region altitudes (e.g., Choosakul et al., 2009).

Now the GPS TEC observations have been used widely to study the acoustic gravity waves and infrasonic waves in the ionosphere and their propagation during extreme weather and space weather events such as tsunamis, earthquakes, solar eclipses and major geomagnetic storms that produce gravity waves and TIDs at high latitudes (e. g, Afraimovich et al., 1998, 2000, 2013; Dasgupta et al., 2006; Komjathy et al., 2016). In the recent past, it is shown that GPS TEC can be used as a effective tool to study the Rayleigh surface waves and Rayleigh wave induced acoustic waves (also known as seismo-traveling ionospheric disturbances (STIDs)) in the ionosphere using travel time analysis from epicenter. If vertical motion is large, they also can generate gravity waves (due to buoyancy) and can propagate to ionosphere. Generally, there is also a good correlation between the magnitude of earthquake and amplitude of TEC perturbation (e.g., Astafyeva et al., 2013; Bagiya et al., 2017). Now several investigations have been made in the past during major earthquakes using GPS TEC including 2011 Tohoku earthquake in Japan and 2004 Sumatra earthquake in Indonesia to understand their coupling mechanisms. The ground and space based GPS TEC observations during 25 April 2015 Nepal earthquake (also referred to as Gorkha earthquake) suggest that two modes exists namely (a) Rayleigh waves with high velocity of ~2.5 km/s and above and (b) Acoustic gravity waves at a velocity range of 1.0-1.2 km/s and periods in the range of few 10s of seconds to few minutes (e.g., Reddy & Seemala, 2015; Tulasi Ram et al., 2017). Though these waves were detected very well in the southern side of the epicenter, interestingly, these waves were not detected in the North-West and Northern side of the epicenter. Based on this, they surmised that surface rupture could be mainly towards southern side than northern side. Sunil et al. (2017), on the other hand, suggested that one of the reasons for this asymmetry could be due to coupling of earth's magnetic field with the acoustic wave. But SAMI2 simulations showed that ionospheric response can be asymmetric due to the changes in the inclination angle of the Earth's magnetic field that causes more wave perturbation in the northern side than southern side of the epicenter even though symmetric wave propagation on north-south direction is assumed (Joshi et al., 2017). Maruyama et al.

(2012) have investigated many ionograms at different stations during the time of earthquake and suggested that Rayleigh wave and acoustic wave signatures can be detected in the ionograms in the form of Multiple Cusp Signatures (MCS) in the ionograms. However, it may be mentioned that these signatures are mainly seen only during daytime. They used numerical simulations to prove that acoustic and gravity waves do produce such 'wiggles' in the ionograms. They also suggested that these 'wiggles' can be seen more clearly at higher inclination angles than at lower inclination due to the fact that earth's magnetic field perturb these waves more efficiently at high inclination angles than at lower inclination angles.

Recent studies have indicated that ionospheric disturbances caused by short period Rayleigh waves couldn't produce appreciable perturbation in the GPS TEC as wavelength of the induced Rayleigh wave is much less than the ionospheric slab thickness. However, investigations have suggested that such short period Rayleigh waves can be measured using fluctuations in the Doppler shift by Doppler sounding technique in HF radio wave reflection. But, Doppler shift of the HF radar system can't provide altitude information as it is limited by its operating frequency. This can be overcome by using rapid run ionograms (high resolution) to study the infrasonic wave signatures in the ionograms (e.g., Chum et al., 2016). Wiggles in the ionograms in the upper E region or F1/F2 region during the time of earthquake are believed to be caused by Rayleigh wave induced acoustic gravity waves. Due to advent of GPS technique, now several GPS/GNSS receivers are deployed across the globe to study the ionosphere dynamics and their variabilities which are linked to earthquakes. International GPS stations (IGS) have been setup to monitor the movement of the plate tectonics as well as TEC count in the ionosphere. Advantage of dense GPS receiver network is to provide high spatial and temporal resolution maps based on line of sight TEC which is integrated from the receiver to the GPS satellite location at every 30sec. While GPS receivers provide horizontal propagation of TEC perturbations, it is not easy to identify the altitude at which these perturbations are amplified strongly. Ionosondes, on the other hand, can be used to identify the altitude variation of these density perturbations. But combining both GPS receivers and ionosonde can provide both altitude and spatio-temporal variation of Rayleigh and acoustic gravity waves generated due to seismic activity.

In this paper, we present results on co-seismic ionospheric disturbances (CIDs) using ground based ionosonde located at Allahabad near anomaly crest region along with few IGS GPS stations in India on 25 April 2015 Gorkha Earthquake. The near field CID is excited by co-seismic vertical crustal displacement which propagates as acoustic wave. These CIDs can be detected in the vicinity of the epicenter. This earthquake is largest earthquake since the 1934 Bihar-Nepal earthquake over Himalayan region (seismic moment magnitude (M_w) =7.8). Since Allahabad station is nearly ~400 km away from Nepal earthquake, it is possible to observe the co-seismic signatures in the ionospheric density structures over Allahabad. To verify this, we analyzed or scaled the ionograms at iso-frequencies and iso-altitudes at high spatial resolutions in addition to foF2 (MHz) and h'F (km) to identify seismic signatures in the ionosonde observations. Usually, the iso-frequency and iso-height analysis are utilized to study acoustic gravity waves and gravity waves in the ionosphere during solar eclipses (Sauli et al., 2006). The same analysis technique is applied here. We used FFT and wavelet analysis techniques to understand the nature of the perturbations. Several types of CIDs have been identified based on the observed characteristics. Short period CIDs (periods of about few 10s of seconds to 5 minutes) and long period CIDs (periods of about tens of minutes) are frequently noticed in the observations. Their wave forms have been described as 'N-type' waves and inverted 'N' types (e.g., Astafyeva et al., 2009).

2. Data sets and methodology

We use high resolution (~5 minutes) observations of Canadian Advanced Digital Ionosonde (CADI) located at Allahabad (25.43°N, 81.84°E), India during Nepal earthquake (28.147°N, 84.708°E) that occurred at 06:11:26 UT (11:41:26 IST) on 25 April 2015 (M_w7.8) to investigate the response of the ionosphere. In addition, we also analyzed several days prior to and after the earthquake day to identify the peculiar signatures of the ionosphere during the time of earthquake than on control days. Also this day is denoted as geomagnetically quiet day. The Ap index is zero and Σkp is less than 1 on 25 April 2015 indicating that there are no strong geomagnetic disturbances on this day. There is also no geomagnetic storm activity prior to and after the Nepal earthquake. So, it is evident that the observations reported here are not affected by geomagnetic storm activity. Similarly, we have examined the lower atmospheric forcing using Outgoing Long wave

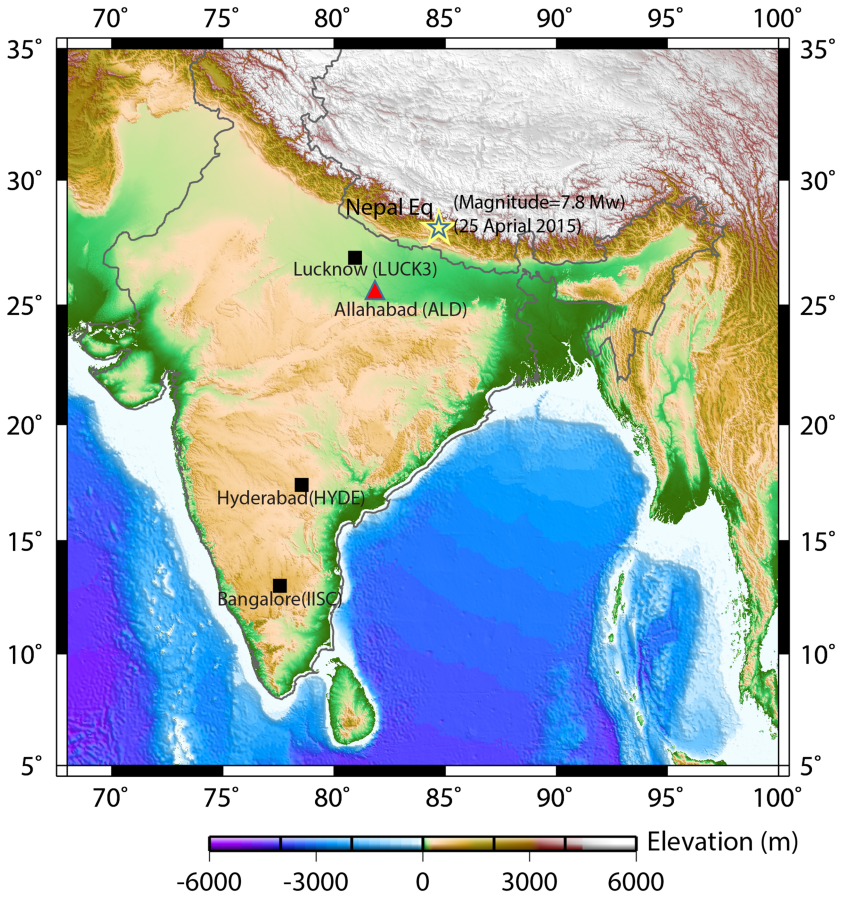

Figure 1. shows the topology map showing ionosonde (delta), IGS GPS stations (square) in India along Indian-Nepal map along with the location of epicenter of the Nepal earthquake.

Radiation (OLR) observations as obtained from NOAA website to check the convective gravity wave activity during the earthquake event. It is noticed that no strong thermal anomalies were observed in the OLR during the time of Nepal earthquake suggesting that there is no strong gravity wave activity in the troposphere. Maurya et al. (2016) also suggested that there is no extreme tropospheric weather events recorded during Nepal earthquake. Also it may be mentioned that Allahabad station is 400 km away from the epicenter of the Nepal earthquake. In addition to CADI, we also use Global Positioning System (GPS) TEC as obtained from few International GNSS Service (IGS) stations in Indian region to study the ionospheric density perturbations. While the GPS TEC has a resolution of 30 seconds, ionogram has a temporal resolution of 5 minutes. But ionosonde can provide altitude information over a given location unlike GPS. So, it will be good to have simultaneous observations together. The GPS satellites transmit radio signals at two frequencies namely 1575.75 MHz (L1) and 1227.25 MHz (L2). The GPS receiver receives these two frequencies, however, with a time delay due to dispersion of the medium. The time delay between these two signals due to this dispersion in the ionosphere is proportional to the line of sight TEC to the GPS satellite. The slant TEC (STEC) can be obtained using this time delay along with more accurate phase information. From the STEC, the vertical TEC (VTEC) can be obtained using mapping function $S_f = \cos\chi$ i.e. VTEC=STEC*cosχ where $\chi = \sin^{-1}\left[\frac{R_E\cos\alpha}{(R_E+h)}\right]$, α is the elevation angle, R_E= Earth's radius, h=350 km to propagate at different velocities. It may be mentioned here that the satellite and receiver bias corrections have been applied to the TEC data using least squares technique to obtain absolute TEC values (See Ma & Maruyama, 2003). Figure 1 shows the location of the sites and the types of instruments used in the present analysis along with the surface deformation information superposed on the map. The ionosonde is typical radar used to sound the ionosphere wherein it sweeps several radio frequencies in the range of 1-20 MHz into the ionosphere and it receives the reflected

signals from the different regions of the ionosphere where plasma frequency equals to that of the radar frequency. Advantage of this system is that it can operate at both single frequency mode as well as ionogram mode (see e.g., Sripathi et al., 2016). The single frequency mode of operation provides line of sight as well as skymap to identify the location of the reflected signal. Using line of sight information from different directions, it is possible to obtain 3 component plasma drifts information using least squares technique. But due to significant noise in the Doppler mode of operation, we could only analyze ionograms instead of Doppler drift information. It may be mentioned that CADI ionosonde can obtain ionograms in either low frequency resolution mode or high frequency resolution mode. Each mode of the operations has both advantages and disadvantages. High frequency resolution mode of observations (~500 frequencies) is mainly used for routine operations (low temporal resolution typically ~15 min) to study low frequency oscillations such as coupling of atmospheric gravity waves, tides and planetary wave activity in the ionosphere. However, in low frequency resolution mode (high temporal resolution), the number of frequencies is usually reduced to nearly half to that of high frequency resolution mode. Here, we present only low frequency resolution ionograms (~200 frequencies) which provides high temporal resolutions (typically ~5 minutes) to investigate the seismic signatures in the ionosonde. It may be noted that high temporal resolution (~5 minutes), however, yields poor altitude information to a certain extent in the ionosonde. The idea to use both GPS and ionosonde data sets in the present analysis is to study both altitude and latitude propagation of the acoustic waves induced due to Rayleigh waves in the ionospheric density during this Nepal earthquake.

3. Observations

The Nepal earthquake is caused by the on-going continent-continent collision between Indian plate and Eurasian plate. The collision has produced the Himalayan Mountains and Tibetan Plateau. The northward underthrusting of India beneath Eurasia generates frequent earthquakes and consequently makes this area one of the most seismically hazardous zone on the earth. A magnitude 7.8 earthquake occurred on 25 April 2015 at 06:11:26 UT (11:41:26 LT) with an epicenter 77 km (48miles) northwest of Kathmandu, the capital city of Nepal. This earthquake became so destructive due to both the shallow depth (15 km) and the fact that Kathmandu lies in a basin filled with ~600m of soft sediment. The sedimentary basins can have a large effect above them on the ground motion. It is known that seismic waves travel faster through the rigid and crystalline rocks but it slows down dramatically when it enters into the sedimentary basin. This increases the amplitude of the earthquake waves within the basin. In addition, the sharp density contrast of the soft basin rocks with surrounding material can cause waves to reflect and trap energy in the basin for an extended period of time. This extends the duration of shaking thus leading to the huge damage to property and human losses (e.g., Kawase & Aki, 1989). Though it produced several aftershocks, we present our results only for the main shock. Figure 2(a-c) shows the displacement of three components namely east-west, north-south and vertical as obtained from seismometer data at Hyderabad station during 25 April 2015. X-axis shows the time in seconds, while y-axis shows the displacement in nanometers. It can be seen that primary wave (P-wave) is observed first followed by S-wave at 06:11:26 UT. The surface waves are seen after a delay of few 10s of sec.

Figure 3(a-b) shows the diurnal variation of (a) foF2 (MHz) and (b) h'F (km) during Nepal earthquake on 25 April 2015 and mean and its standard deviation using 5 geomagnetic quiet days. The figure suggests that foF2 values were higher and fluctuations were more during the time of earthquake as compared to quiet day values. Also the observations suggest that h'F (km) is higher and having several perturbations during earthquake time as compared to quiet day value. Based on this figure, it can be suggested that foF2 (MHz) is higher during 25 April 2015 and the difference of foF2 (MHz) between the earthquake day and quiet day suggest that there is a strong density perturbations on earthquake day at 6:45 UT and 08:15 UT. Figure-4(a-c) shows portion of (a) foF2 (MHz) on 25 April 2015 along with mean and standard deviation of 5 international quiet days namely 07, 08, 12, 28 and 29 during April 2015, (b) deviations or fluctuations in the foF2 (MHz) at the time of earthquake on earthquake day with reference to mean of the quiet days and (c) its wavelet analysis using the fluctuations of foF2 as shown in figure-4b. The figure suggests that there are large density perturbations during the time of earthquake and after wards. Several peaks in density perturbation is noticed after 006:00 UT. It can be seen that there are wave like oscillations in the fluctuations in foF2 with peak amplitudes after 6.5 UT. The wavelet analysis on foF2 shows the dominant frequencies at 0.7 mHz immediately after earthquake and 0.9 mHz with a delay.

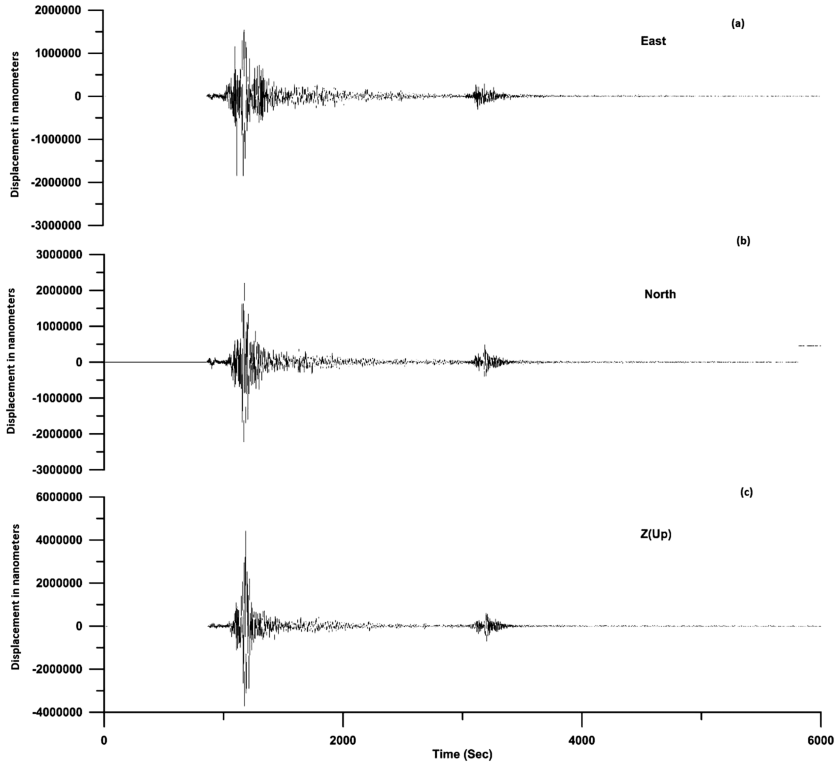

Figure 2. (a-c) shows the displacement (in nanometers) of (a) East-west, (b) North-south and (c) Up-down (vertical) components as recorded at Hyderabad seismometer station on 25 April 2015.

3.1. Ionogram 'cusp' signatures during Nepal earthquake on 25 April 2015

In order to show the actual ionogram images to study ionogram 'cusp' signatures at the time of earthquake on 25 April 2015 at Allahabad, we presented few ionograms between 11:40-11:55 IST (06:10-06:25 UT) in Figure-5(a-d). It may be noted that quality of these ionograms are not very good due to noise and lack of strong return signal but keen observations suggest that there are some 'cusp' regions in the ionograms (as

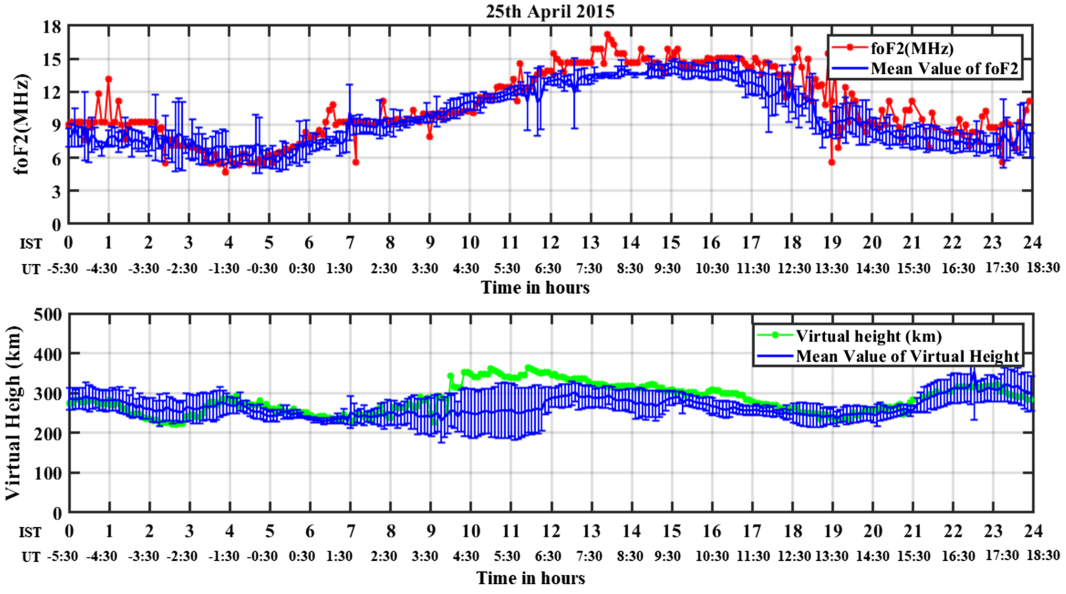

Figure 3. (a-b) shows the diurnal variation of (a) foF2 (top) and (b) h'F (km) (bottom) on 25 April 2015 along with mean and standard deviation of geomagnetically quiet days during April 2015

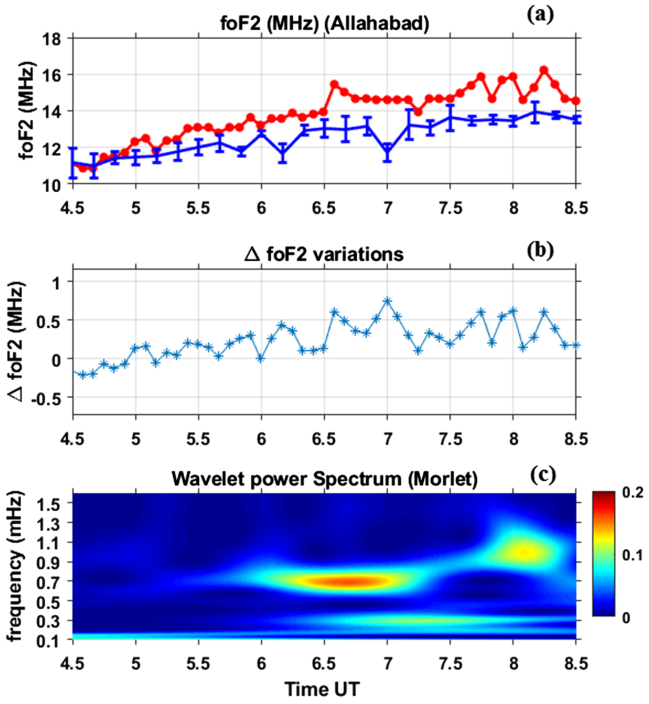

Figure 4. (a-c) shows the temporal variation of (a) foF2 (MHz) on earthquake day (red) and mean and standard deviation of geomagnetically quiet days (blue) of April 2015 and (b) fluctuations in foF2 (MHz) with reference to control days at the time of earthquake on 25 April 2015, (c) wavelet analysis on the fluctuations in foF2 (MHz).

highlighted in 'red' circle) which may be caused due to modulation of ionization by Rayleigh wave induced acoustic waves on 25 April 2015. Existence of such 'cusp' regions during passage of Rayleigh wave induced acoustic gravity waves are thoroughly discussed using both observations and simulations in a paper by Maruyama et al. (2012). It is believed that these 'cusp' regions are nothing but density modulation by these acoustic gravity waves. As we believe we have seen possible 'cusp' or 'wiggle' signatures in the ionograms over Allahabad, we try to investigate the density modulations by studying iso-density and iso-height variations at the time of earthquake on 25 April 2015.

3.2. Iso-density variations and their wavelet analysis

Figure-6(a-b) shows the temporal variation of altitude variation of iso-frequency values at (a) 4, 5 and 6 MHz (left plot) and (b) 7 and 8 MHz (right plot) frequencies. Here the black color indicates the running mean. Actual height fluctuations at these iso-frequencies are also shown in the figure with different colors. It may be mentioned that the iso-density and iso-height scalings were performed to identify the acoustic gravity waves and gravity waves during solar eclipses. Such methods have been used extensively to investigate propagation of acoustic gravity waves or gravity waves in the ionosphere elsewhere. So, this scaling is very useful to identify the density modulations which are not able to identify in foF2 and h'F (km). Also it may be mentioned that these virtual heights as scaled at iso-frequencies are sometimes artificially uplifted by a constant value for better visualization. But we have not uplifted the height artificially here. The observations show that strong fluctuations at shorter scales during 06:00-07:00 UT were noticed. This time coincides with the onset time of Nepal earthquake. The larger scale fluctuations that are seen at higher frequencies (at higher heights) in the figure-6b prior to earthquake could be due to other dynamical processes such as semi-diurnal tidal and meridional winds influence.

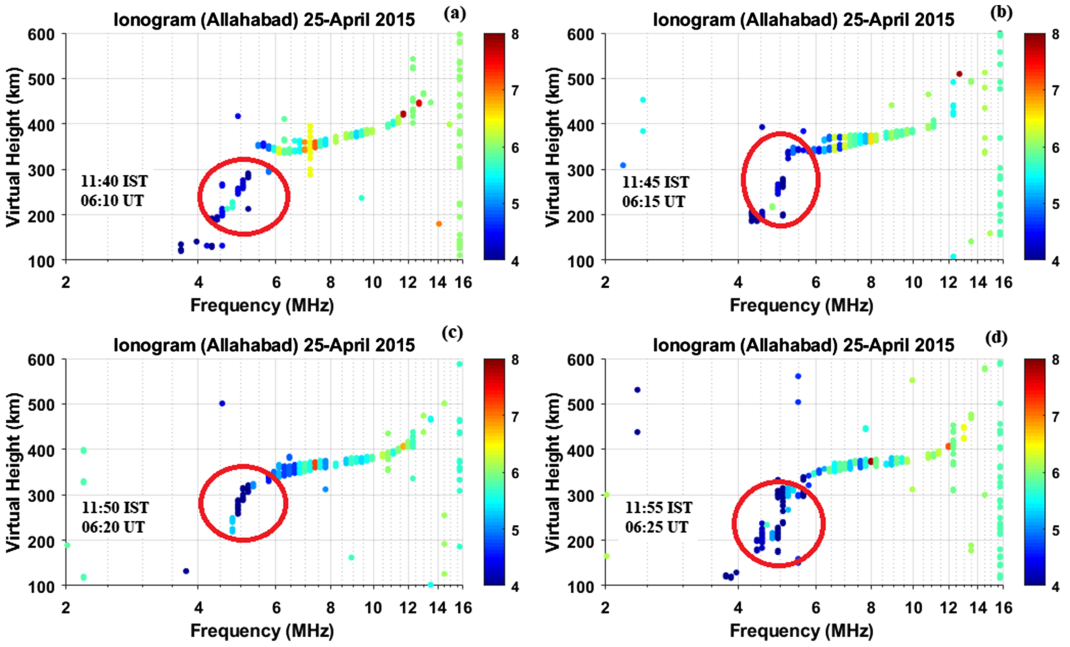

Figure 5. (a-d) shows the standard ionogram images at the time of earthquake on 25 April 2015. The color bar indicates the signal strength of the received echoes.

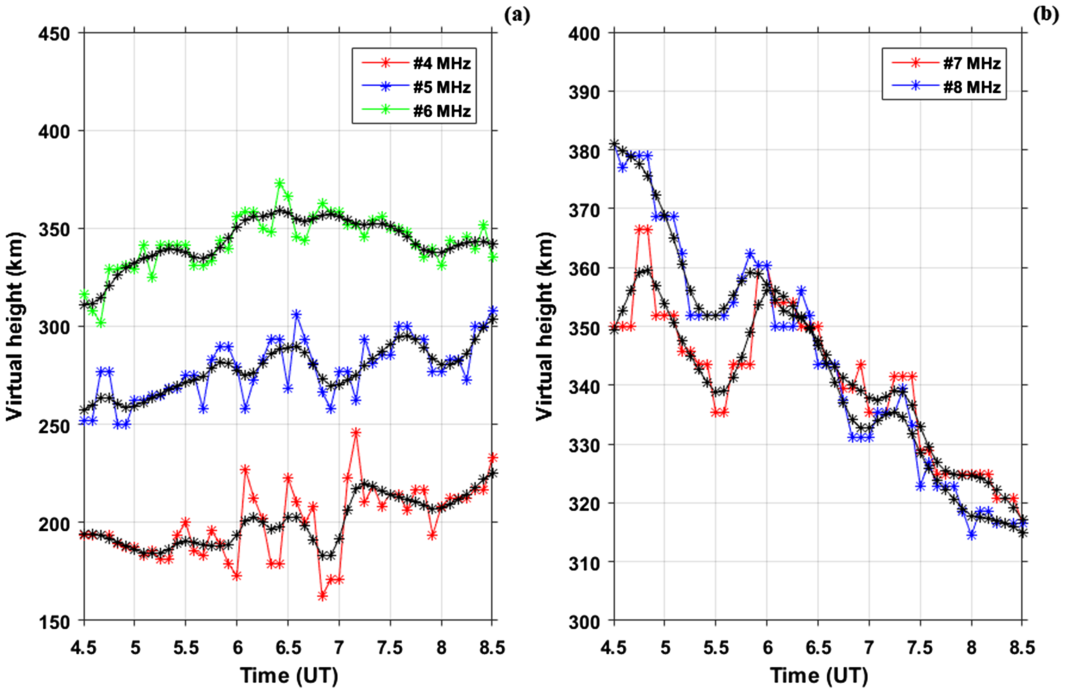

Figure 6. (a-b) shows the temporal variation of virtual height at iso frequencies at (a) 4-6 MHz frequencies (left) and at (b) 7-8 MHz (right) on 25 April 2015 and their running mean shown in black color.

Figure-7(A-C) shows the (a) virtual height variations scaled at iso-densities 4, 5 and 6 MHz (blue) along with mean of five geomagnetically quiet days (black), (b) the difference of quiet day mean and on 25 April 2015 (middle panel), (c) (bottom panel) wavelet analysis on the difference in the virtual height between quiet day mean and 25 April 2015 during 10:00-14:00 IST (04:30-04:30 UT). It may be mentioned that the Morlet wavelet analysis presented here and subsequent analysis were performed based on the technique mentioned in Torrence and Webster (1999). The periodogram analysis suggests that height oscillations at shorter periods (high frequencies) were more dominant during 05:30-07:30 UT (11:00-13:00 IST (Indian Standard Time (IST) = UT+5.5)). The dominant short period or high frequency oscillations were found to be at ~1.3 mHz (12 min), 0.9 mHz (18 min) and ~0.5 mHz (30 min). While the 1.3 mHz (12 min period) frequency could be associated with Rayleigh wave induced acoustic waves, other two periods could be related to gravity waves which might have generated during Nepal earthquake close to epicenter. It is believed that these atmospheric gravity waves or acoustic gravity waves are generated at the surface of the earth due to Rayleigh waves during earthquake which propagates to higher altitudes and perturb the ionized medium through collisions. The gravity wave effects can be seen close to epicenter.

3.3. Iso-height variations and their wavelet analysis

Figure-8(a-b) show the (a) density variations without any trend removal and (b) density variation after trend removal based on constant virtual heights as scaled at every 5 km from 180 to 330 km during 04:30-08:30 UT to investigate the density perturbations at different altitudes during Nepal earthquake. Figure-8c shows the wavelet analysis of a typical height at 245 km. It may be mentioned that we applied 2-point smoothing to identify the waves. Also it may be mentioned that these virtual heights scaled at iso-frequencies are artificially uplifted by a constant value for better visualization. The Figure-8a suggests that there are several types of density fluctuations are visible. Initially the density variations as seen in the figure appear to be due to slowly descending layer structures. Here the layer starts first at higher altitude but as time progresses, the layer descending to lower altitudes. The phase velocity of this descending is very small (~7.7 m/s). In the later times, we also noticed another such descending layer structure in density variations which are weak. However, third density structure that is seen at 07:00 UT appears to be propagating to upward from below. This upward propagating structure seems to be caused by Rayleigh wave induced acoustic wave. The wavelet analysis for a height at 245 km is shown in the Figure-8c (right) which indicates that there exist short period

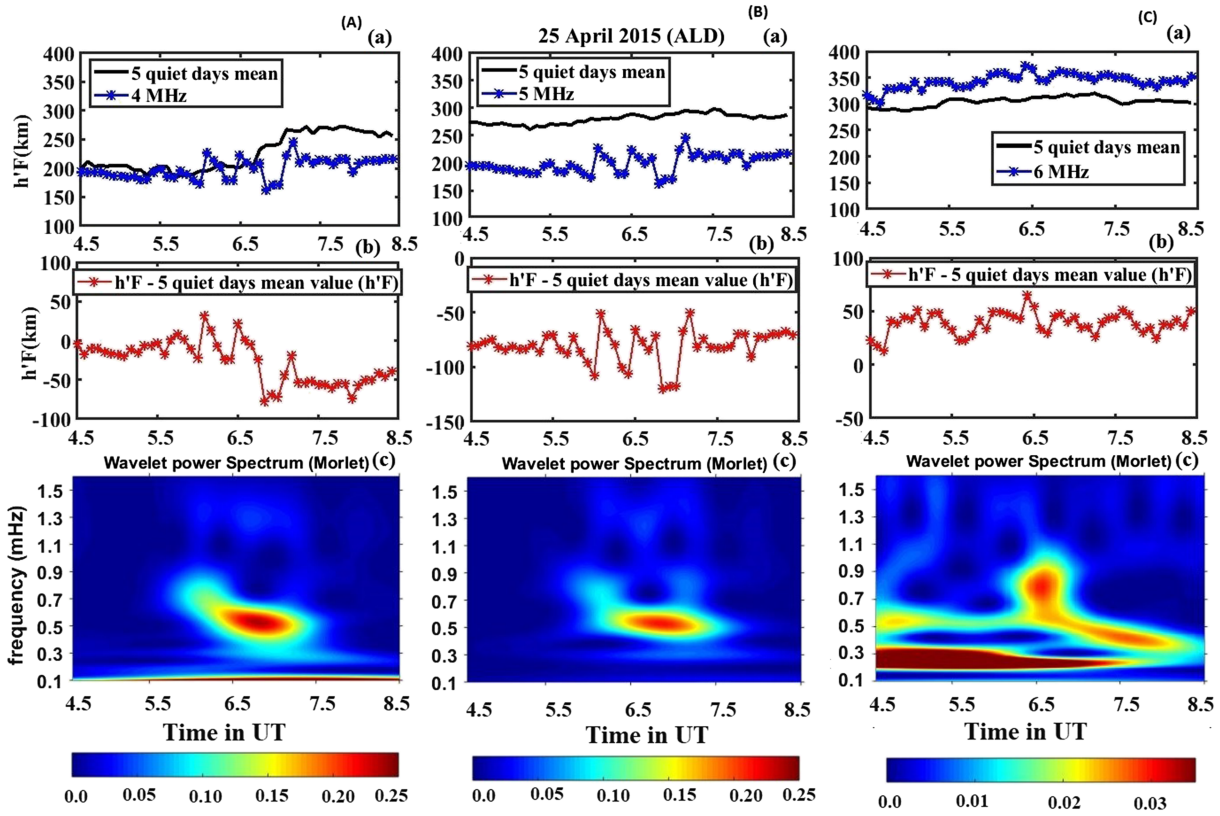

Figure 7. (A-C) display (a) temporal variation of virtual height at 04:30-08:30 UT (10:00-14:00 IST) on 25 April 2015 along with quiet day mean and (b) their temporal variation in difference between these two heights, (c) wavelet analysis applied to the fluctuations in the virtual height difference as shown in (b) at 4 MHz, 5 MHz and 6 MHz respectively

waves with wave frequency in the range of 0.7-1.5 mHz. These periods correspond to 11 minutes to 25 minutes. It is believed that these periods could be associated with Nepal earthquake as such periodic oscillations were not seen on other quiet days.

3.4. GPS TEC observations of seismic signatures and their propagation

Figure-9(a-b) shows the temporal variation of (a) STEC (TEC Units) and (b) filtered STEC as obtained using PRN#26 [PRN=Psudo Random Noise] at Lucknow, Hyderabad and Bangalore stations. It may be noted that the TEC fluctuations due to earthquake are seen mostly in PRN#26 and accordingly we are showing time history of TEC as recorded by this satellite only. While other satellites also observed such TEC increase, we have not shown here. In the figure, it can be seen that there is a sudden increase of TEC near 06:30 UT. This increase is not only seen at one station but is seen in all three stations. As the Lucknow station experienced weak increase, the enhancement is not visible properly. But the TEC fluctuations can be seen in filtered TEC which will be discussed next. Also can be noticed is the delay of this increase from one station to other station. It is possible for us to obtain the phase velocity of this wave using this delay time. In order to extract only fluctuations to estimate the propagation velocity, we applied high pass filter at 2-10 mHz to the TEC data for all the stations as shown above. The filtered data is plotted in Figure-9b. Also it may be mentioned that these TEC values are artificially uplifted in both plots by a constant value for better visualization. Figure-9b shows the increase of TEC during the time of Rayleigh wave or acoustic wave propagation. Also it is interesting to see that the TEC perturbation is propagated from one station to other with a time delay. Based on the distance between the epicenter of the earthquake and GPS receiver location and their location with respect to epicenter, the velocity works out to be of the order of 500 m/s to 1.0km/sec. The velocities of the waves are estimated as follows: we identified the IPP (ionospheric pierce point) latitude and longitude of the TEC and its time when we see the earthquake signature. We also know the epicenter of the earthquake. Now based on these, we estimated the distance using the following website: http://www.nhc.noaa.gov/

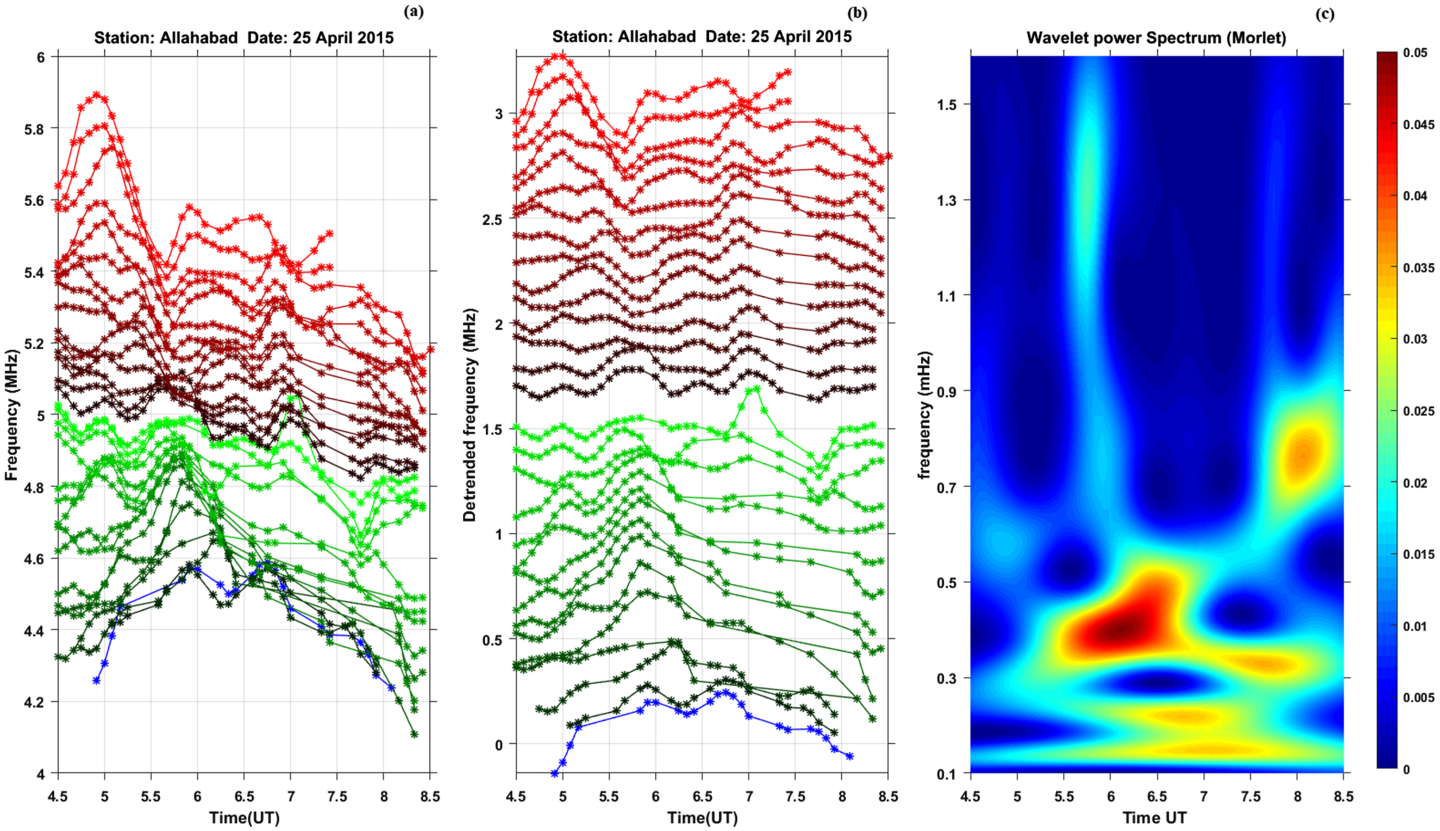

Figure 8. (a-c) display (a) temporal variation of the frequency (density) variations on 25 April 2015 as scaled at isoheights between 180-330 km with 5 km altitude resolution, (b) detrended frequency (density) variation and (c) wavelet analysis on the detrended frequency at 245 km.

gccalc.shtml. The estimated epicentral distances are 414 km, 817 km and 1188 km respectively after a time delay of 11.55, 17.06 and 19.04 minutes for PRN#26 for Lucknow, Hyderabad and Bangalore stations. Now the estimated velocities are in the range of ~0.5-1.0 km/s. This velocity is in the range of Rayleigh wave induced acoustic wave velocities. Also we notice that higher velocities are away from the epicenter. Several studies have been already made to understand the coupling of lithospheric processes such as Rayleigh waves, acoustic gravity waves, seismo traveling ionospheric disturbances and detection of

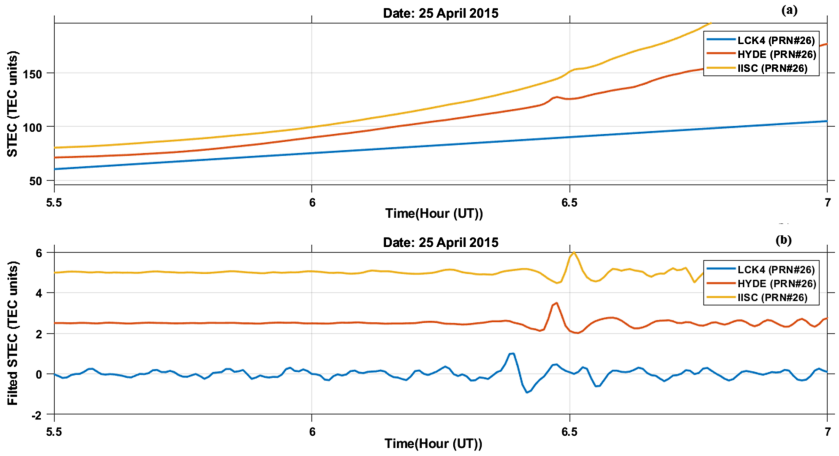

Figure 9. (a-b) shows (a) the temporal variation of GPS TEC at IGS stations namely Lucknow, Hyderabad and Bangalore using PRN no#26 on 25 April 2015 and their (b) high pass filtered TEC at 2-10 mHz during the 05:30-07:00 UT on 25 April 2015.

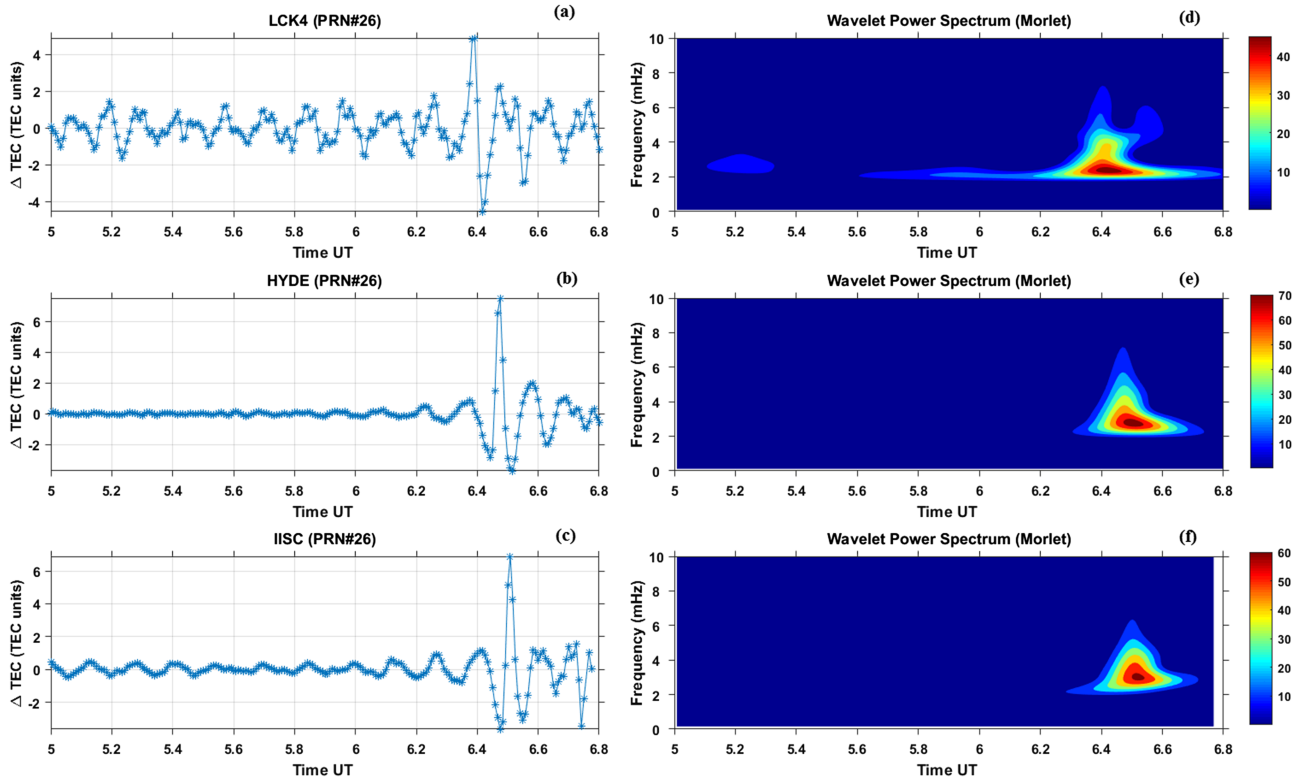

Figure 10. (a-f) shows the (left) temporal variation of high-pass filtered TEC at 2-10 mHz using PRN no#26 on 25 April 2015 as recorded by (a) Lucknow (LCK4), (b) Hyderabad (HYDE) and (c) Bangalore (IISC) and (right) their wavelet analysis in (d-f).

atmospheric gravity waves using GPS TEC observations alone. Now the temporal variation of filtered TEC data at PRN#26 as recorded by (a) LCK4, (b) HYDE and (c) IISC (left) and their wavelet analysis (right) is shown in Figure-10(a-f). It can be seen that there exists a nice periodic oscillations in the range of 2-4 mHz in all the stations data. But it can be seen that the periods are shifted in time from top to bottom. The results also suggest that Lucknow which is near to the epicenter of the earthquake has dominant lower frequencies, while other two stations show that they are relatively dominant at higher frequencies. Here we make use of GPS TEC observations to connect these observations with that of the ionosonde results.

4. Results and Discussion

We have seen that the results presented in the previous section show the signatures of co-seismic waves in ionosonde located at Allahabad near anomaly crest as well as from GPS TEC observations based on PRN#26 as recorded from GPS receivers located at Lucknow, Hyderabad and Bangalore on 25 April 2015 Gorkha Earthquake. The filtered TEC observations at 2-10 mHz suggest their southward propagation from epicenter with a velocity of 500 m/s to 1.0 km/sec which is in the range of acoustic gravity wave speeds in the ionosphere. The Rayleigh wave shock at the surface induces infrasonic waves which travels to the ionosphere and produces density perturbations in TEC and cusp signatures in the ionosonde observations. The advantage of TEC observations is to have spatial propagation using travel-time diagrams, while the disadvantage of the GPS observation is that it can't provide information of wave propagation on short periods and on altitude. But the short period Rayleigh wave disturbances can be measured using fluctuations in the Doppler shift by Doppler sounding technique in HF radio wave reflection. It is found one-to-one correspondence between Doppler signal and seismic waves (e.g., Yuen et al., 1969). However, Doppler shift of the HF radar system can't provide altitude information as it is limited by its operating frequency. This can be overcome by using rapid run ionograms (high resolution) to study the infrasonic wave signatures in the ionograms. The high resolution ionosonde observations as presented above show wave perturbations possibly linked to acoustic and atmospheric gravity waves during the time of earthquake. It is known that the near field that is excited by co-seismic vertical displacement propagates as acoustic waves and gravity waves in the

ionosphere. These acoustic waves and gravity waves can be detected in the vicinity of the epicenter as earthquake triggers several types of waves at the surface of the earth which propagate to higher altitudes to produce ionized density perturbations. But they can be distinguished based on their velocities, periods and types of propagation. While acoustic waves propagate longitudinally at higher frequencies, gravity waves propagate in the form of transverse waves at relatively smaller frequencies. As Mw 7.8 Nepal earthquake is largest since the 1934 Bihar-Nepal earthquake from the Himalayan region, it is expected that co-seismic signatures exist in the ionospheric density structures over Allahabad. However, it depends on how accurately we can extract the information. Any atmospheric waves generated in the vicinity of Nepal earthquake can be detected at Allahabad since Allahabad station is nearly ~400 km away from the epicenter. Keeping this, we scaled the iso-frequencies and iso-altitudes at high spatial and temporal resolutions in addition to foF2 (MHz) and h'F (km) to identify seismic signatures in the ionosonde observations. The periodogram and wavelet analysis on the iso-frequency and iso-altitudes suggest that there are strong density fluctuations in the ionosphere during the time of earthquake. However, such density fluctuations are not seen on other days. Several types of waves such as short and long period waves have been identified in our analysis. The GPS TEC observations show short period waves (periods of about few 10s of seconds to 5 minutes) which are fast acoustic waves induced by Rayleigh waves. However, long period waves (periods of about few tens of minutes to less than an hour) which are conventional atmospheric gravity waves or buoyancy waves are noticed in the ionosonde observations very clearly. This could be possibly due to the fact that Allahabad is located close to epicenter which can see both Rayleigh wave induced acoustic waves as well as gravity waves. Maruyama et al. (2012) have investigated the ionogram images for cusps in total of 43 events as obtained at 5 ionosonde stations in Japan with seismic activity magnitude of earthquakes of 8.0 or greater. Their results suggest that MCS in ionograms provide snapshot of vertical disturbances induced by acoustic waves. They found 7 min of offset delay after the earthquake which is consistent with the propagation time of acoustic wave from the ground to ionosphere. They found vertical disturbance wavelength in the range of 10-30 km corresponding to wave period of 20-50 sec. The acoustic waves triggered by Rayleigh wave is believed to be interacting with electron density distribution through collisions between ions and neutrals leading to MCS signatures. They further suggested that Rayleigh waves detected in TEC observations and ionogram traces are not exactly same. It is believed that wave period of disturbances that causes MCS are shorter than that of TEC measurements. As the phase of the perturbation changes at short distances for fast waves, they mayn't cause appreciable perturbations in TEC but can be seen in ionograms. On comparing both observations and simulations, it is noticed that cusp regions with large amplitude is seen near F1 region where density gradient is gradual and smooth than at F2 region where density gradients are large and steepest and could be related to earthquake. But it is possible that the ionospheric density can also be affected by forcing from below such as atmospheric waves and tides and forcing from above such as solar flux and geomagnetic storms (e.g., Forbes et al., 2000; Rishbeth & Mendillo, 2001; Chau et al., 2009, 2010). Accordingly, we examined all the possible forcings such as lightning and thunderstorms through OLR observations and geomagnetic activity through Ap and kp indices which may also cause periodic waves in the ionosphere during this period and we found that there are no major disturbances in the troposphere. Similarly, we also examined the geomagnetic activity levels on 25 April 2015 and found that there is no geomagnetic activity. Accordingly, we consider that the wave periods as seen our analysis on 25 April 2015 is linked to the seismic activity.

Dasgupta et al. (2006) have investigated the ionospheric perturbations due to Sumatra-Andaman earthquake (Mw 9.15) that launched Tsunamis during 26 December 2004 using GPS And Geo-augmentation Navigation (GAGAN) network over Indian region. They found significant TEC perturbations in the range of 1.5-2 TEC units after 45 min. The disturbance was later found to propagate northwestward direction from the epicentre. They interpreted this as due to Traveling Ionospheric Disturbances propagated from the earth's surface. The results during Nepal earthquake suggest that two modes namely Fast acoustic waves induced by Rayleigh waves which are having high velocity ~2.5 km/s and Acoustic gravity waves which are in the velocity range of 500-1000 m/s with periods in the range of few 10s of seconds to few minutes were predominantly seen propagating to Indian low latitudes. Though these waves were detected very well in the southern side of the epicenter, but interestingly, these waves were not detected in the North-West and Northern side of the epicenter. Some other studies have suggested that the coupling function between earthquake induced acoustic wave and geomagnetic field plays significant role in creating asymmetry in

ionospheric perturbation in the north-south direction through the surface deformation is symmetric in the north-south direction (Heki & Ping, 2005; Maruyama et al., 2011; Kherani et al., 2009). Maruyama et al. (2017) suggested that the 'wiggles' in the ionograms can be seen more clearly at higher inclination angles than at lower inclination due to the fact that earth's magnetic field perturb these waves more efficiently at high inclination angles than at lower inclination angles. But GPS TEC observations presented for the Nepal earthquake suggests that wave perturbations were in fact more predominant in the southern side of the epicenter than in the northern side. SAMI2 simulations, on the other hand, suggest that this asymmetry could be due the changes in the inclination angle of the earth's magnetic field that cause more wave perturbation in the northern side than southern side of the epicenter. While some studies have suggested that TEC amplitude can be enhanced in the northern side of the epicenter, other studies have showed opposite to it. Catherine et al. (2017) also have investigated the Nepal earthquake using GPS TEC observations and suggested that these Rayleigh wave induced acoustic waves are not propagated to northern latitudes but they propagated to southern latitudes which is in agreement with Reddy and Gopi (2015) but in contrast to Joshi et al. (2017) modeling work. They suggested that their observations are in agreement with rupture propagation in the direction of East to South-East. Since rupture propagated to south direction, it is possible that TEC perturbations are also showing their propagation towards southern direction. But Joshi et al. (2017) has considered that rupture is uniform in the north and south direction. We believe that if rupture propagation can be factored in SAMI2 model, the results could be similar to Catherine et al. (2017). Hegai et al. (2006) have also investigated the propagation of atmospheric gravity waves prior to earthquakes. They suggested that ionospheric Joule heating produced by seismogenic electric field of short duration can generate these gravity waves. They further suggested that these gravity waves perturb more in the north-south of the epicenter than east-west of the epicenter. Our results of GPS TEC also show the southward propagation from the epicenter and agree with the rupture propagation direction but ionosonde results are not showing any such signatures possibly due to poor temporal resolution. Also since ionosonde only looks vertical, we can't say much. However, altitude fluctuations suggest that lower altitudes are showing stronger fluctuations of these waves than higher altitudes. It is suggested that such strong fluctuations can be seen mostly at lower altitudes but they can suffer attenuation at higher altitudes (see Yuen et al., 1969).

Liu and Sun (2011) have investigated the Tohoku earthquake on 11 March 2011 (Mw 9.0) using concurrent and collocated measurements of seismometers infrasonic system, magnetometer, HF-CW Doppler sounding system along with GPS receivers to detect the ionospheric disturbances triggered by seismic waves. The results suggest that no time delay between infrasonic waves and seismic waves which suggest that acoustic and/or gravity waves in the atmosphere near the Earth's surface can be immediately triggered by vertical ground motions. The acoustic wave speed of 1.0 km/s as estimated using arrival time and the epicenteral distance suggest that infrasonic waves are mainly induced by Rayleigh waves which are in agreement with other observations and theory. The positive perturbation in the GPS TEC during seismic event is investigated by Heki and Ping (2005). They suggested that the positive pulses emerged after ~10 min of earthquake propagated horizontally with velocity of ~1 km/s in the ionosphere. They believed that these waves are excited by co-seismic upliftment of the surface and propagated as upward propagating compressional wave of the atmosphere which gradually refracted in the ionosphere to propagate horizontally at an altitude of 300 km. Wavelike perturbations in the ionospheric critical frequency foF2 as induced after the Ms 8.1 Samoa earthquake in the Pacific Ocean on 29 September 2009 is investigated by Hegai et al. (2011). They observed such perturbation after nearly 1.2 hours of the shock and these perturbations were present for ~3 hours above the station. The amplitude of their wave is found to be 20% higher than the average quiet time foF2. When they compared these observations with that of well-known Alaskan earthquake on 28 March 1964 (Ms. 8.4) using Stanford station, they showed similar wave like variations in foF2. These results are in agreement with the acoustic gravity wave propagation after earthquake. Our observation of foF2 on Nepal earthquake shows similar wave like oscillations and these oscillations are much above the quiet time variation of foF2 suggesting that we are observing seismic signatures in the foF2. The altitude at which we notice the density perturbation is in the range of 180-250 km which is below the F2 layer height. Also the perturbation amplitude is increased by a factor of 10^4-10^5 at the bottomside of the F layer. The observations presented here suggest that short period wave doesn't propagate to very higher altitudes as they are severely attenuated. These observations are in support of the Doppler observations by Yuen et al. (1969) where they have shown that 5 MHz frequency (short period waves with 20-25 seconds) reaches the 200 km earlier but 10

MHz frequency (long period waves with 2 minutes) reaches the 300 km at much later time indicating that shorter periods can be seen mostly at lower F region while larger period waves can be seen at higher altitudes at a later time. These results were in agreement with theoretical pressure oscillations. Sun et al. (2016) have investigated the ionospheric density perturbation induced by 25 April 2015 Nepal earthquake using FORMOSAT-3/COSMIC (F3/C) and suggested that ionospheric density is perturbed by quake induced acoustic wave speed of 800 m/s near peak altitude (hmF2). They observed that vertical wave length of 150 km in density perturbation which is significantly larger and also the hmF2 is uplifted by nearly 30 km within a min. A comparison using radar and GPS TEC after Tohoku earthquake (Mw 9.0) suggests that there are significant discrepancies between these two observations in detecting density perturbation (e.g., Ogawa et al., 2012). Their analysis indicates that waves with speeds of 6.7-1.8 km/s could be noticed in radar but it is not noticed in TEC, while slow acoustic waves with phase velocity of 1.3-0.7 km/s as noticed in TEC are not detected in radar. Based on these results these authors indicated that GPS TEC could be sensitive to electron density distribution mainly at 250-350 km, while the radar could detect the plasma disturbances at 250 km and it can't detect if the acoustic waves propagated to higher altitudes.

Saito et al. (2011), on the other hand, have investigated GPS TEC during 2011 Tohoku earthquake with magnitude of 9.0 and suggested that the ionospheric variations are having dominant frequency of oscillations at 4.5 mHz and minor frequency of oscillations at 3.7 mHz and 5.3 mHz. They suggested that these periods are in the range of acoustic resonance between the ground and lower thermosphere. These resonant oscillations were also accompanied by TEC depletions. It is believed that when acoustic waves propagate up into the ionosphere vertically, some of these waves are reflected back from the lower thermosphere and interact with the upward propagating waves. It is believed that some of these waves are leaked upward and causes ionospheric perturbations at these resonant frequencies. This is very clearly seen in our GPS TEC observations where we observe waves between 2-4 mHz and some of those waves fall into this acoustic resonance range. Shinagawa et al. (2007), using simulations, have suggested that these resonance acoustic waves are limited to the vicinity of epicenter due to the fact that these resonances occur mostly by vertical reflection. Interestingly, as we notice that 2-3 mHz frequency at Lucknow station which is prolonged for a long time and is close to epicentre of the earthquake, it is possible that this station could be recording the acoustic resonance. However, we are not able to notice any TEC depletion at this station unlike Tohoku earthquake where they have noticed TEC depletion for an hour or more.

In the ionograms, the 'cusp' signatures indicate upward propagating acoustic gravity waves as induced by Rayleigh waves. These 'cusp' signatures are indeed believed to be produced by the short wavelength acoustic gravity waves which are much smaller (few 10s of kms) than the thickness of the ionosphere (Maruyama et al., 2016). Since we have seen signatures of such 'cusps' in the ionograms in the present analysis, we believe that we are detecting such acoustic gravity waves at Allahabad. But we need at least 1 minute resolution to investigate further on these wave structures and their vertical propagation characteristics. Finally, while the results presented in this paper are in conformity with previous analysis, combining GPS TEC and ionosonde observations in this work is a new study for this earthquake and these results are very much encouraging. Due to weak scattering points as well as noise from the CADI system, we could not study the Doppler measurements here. In future, we wish to address this issue using better signal processing. We also would like to investigate further using other earthquake events and try to understand the physical processes behind lithosphere-atmosphere-ionosphere coupling and their possible predictions (Heki, 2011; Dabas et al., 2007).

5. Conclusions

We presented high-resolution ionosonde observations (~5 minutes) at Allahabad near anomaly crest location in India along with GPS TEC measurements using Indian IGS stations to study the possible manifestation of co-seismic signatures in the ionosphere following M_w7.8 Nepal Earthquake that occurred at 06:11:26 UT on 25 April 2015. Observation of multiple cusps in the ionograms suggests the possible role of Rayleigh waves and it's induced acoustic gravity waves in modulating electron density in the ionograms at Allahabad station. The GPS TEC show signatures of co-seismic perturbations after the onset of earthquake and are found to propagate to southward with a speed of ~0.5-1.0 km/s. The periodogram and wavelet analysis on iso-density and iso-height suggest the presence of possible acoustic gravity waves and atmospheric gravity

waves in the altitude range of 180-250 km with the periods in the range of 12 min, 18 minutes and 30 minutes respectively in the lower F region. Also our observations show wave like perturbations in the foF2 values having period of 23 minutes indicating density disturbances due to atmospheric gravity waves or buoyancy waves. The results presented here suggest that there could be good coupling between seismic activities triggered acoustic gravity waves and ionized density perturbations in the ionosphere during the co-seismic activity. Further analysis is underway to identify wave signatures of major earthquake events and their possible precursory signatures in the ionosonde observations.

Acknowledgments
The research work presented here is carried out using in-house project 'Coupled of Lithosphere-Atmosphere-Ionosphere-Magnetosphere system (CLAIMs)' at IIG. The authors are thankful to the Director, IIG for initiating this interesting area of research in our institute and extending his kind support and help. Authors also would like to thank WDC geomagnetic data center, Kyoto University, Japan for providing geomagnetic indices and NGDC for providing solar flux data. Authors also would like to thank ftp://cddis.nasa.gov/gnss/data/daily/ for providing GPS TEC data over Indian region. We also would like to acknowledge the INCOIS, Hyderabad for providing seismic data. Partial help of ionosonde data scaling analysis by Ms. Neha Kumari, K.J.Somaiya College of Science and Commerce, Mumbai on few selected days is acknowledged. The GPS data is available openly and can be examined. The processed ionosonde data and GPS data can be accessed at https://doi.org/10.5281/zenodo.3594760.

References

Afraimovich, E. L., Astafyeva, E. I., Demyanov, V. V., Edemskiy, I. K., Gavrilyuk, N. S., Ishin, A. B., et al. (2013). Review of GPS/GLONASS studies of the ionospheric response to natural and anthropogenic processes and phenomena. *J. Space Weather Space Clim*, *3*, A27. https://doi.org/10.1051/swsc/2013049

Afraimovich, E. L., Kosogorov, E. A., Leonovich, L. A., Palamarchouk, K. S., Perevalova, N. P., & Pirog, O. M. (2000). Determining parameters of large-scale traveling ionospheric disturbances of auroral origin using GPS-arrays. *Journal of Atmospheric and Solar - Terrestrial Physics*, *62*(7), 553–565.

Afraimovich, E. L., Palamartchouk, K. S., Perevalova, N. P., Chernukhov, V. V., Lukhnev, A. V., & Zalutsky, V. T. (1998). Ionospheric effects of the solar eclipse of March 9, 1997, as deduced from the GPS data. *Geophysical Research Letters*, *25*(4), 465–468. https://doi.org/10.1029/98GL00186

Afraimovich, E. L., Perevalova, N. P., Plotnikov, A. V., & Uralov, A. M. (2001). The shock-acoustic waves generated by the earthquakes. *Annales de Geophysique*, *19*(4), 395–409.

Artru, J., Farges, T., & Lognonné, P. (2004). Acoustic waves generated from seismic surface waves: Propagation properties determined from Doppler sounding observations and normal-mode modeling. *Geophysical Journal International*, *158*, 1067–1077. https://doi.org/10.1111/j.1365-246X.2004.02377.x

Astafyeva, E., Heki, K., Afraimovich, E., Kiryushkin, V., & Shalimov, S. (2009). Two-mode long-distance propagation of coseismic ionosphere disturbances. *Journal of Geophysical Research, Space Physics*, *114*, A10307. https://doi.org/10.1029/2008JA013853

Astafyeva, E., Shalimov, S., Olshanskaya, E., & Lognonné, P. (2013). Ionospheric response to earthquakes of different magnitudes: Larger quakes perturb the ionosphere stronger and longer. *Geophysical Research Letters*, *40*, 1675–1681. https://doi.org/10.1002/grl.50398

Bagiya, M. S., Sunil, A. S., Sunil, P. S., Sreejith, K. M., Rolland, L., & Ramesh, D. S. (2017). Efficiency of coseismic ionospheric perturbations in identifying crustal deformation pattern: Case study based on Mw 7.3 May Nepal 2015 earthquake. *Journal of Geophysical Research: Space Physics*, *122*, 6849–6857. https://doi.org/10.1002/2017JA024050

Catherine, J. K., Maheshwari, D. U., Gahalaut, V. K., Roy, P. N. S., Khan, P. K., & Puviarasan, N. (2017). Ionospheric disturbances triggered by the 25 April, 2015 M7. 8 Gorkha earthquake, Nepal: Constraints from GPS TEC measurements. *Journal of Asian Earth Sciences*, *133*, 80–88.

Chau, J. L., Aponte, N. A., Cabassa, E., Sulzer, M. P., Goncharenko, L. P., & González, S. A. (2010). Quiet time ionospheric variability over Arecibo during sudden stratospheric warming events. *Journal of Geophysical Research*, *115*, A00G06. https://doi.org/10.1029/2010JA015378

Chau, J. L., Fejer, B. G., & Goncharenko, L. P. (2009). Quiet variability of equatorial E × B drifts during a sudden stratospheric warming event. *Geophysical Research Letters*, *36*, L05101. https://doi.org/10.1029/2008GL036785

Choosakul, N., Saito, A., Iyemori, T., & Hashizume, M. (2009). Excitation of 4-min periodic ionospheric variations following the great Sumatra-Andaman earthquake in 2004. *Journal of Geophysical Research*, *114*, A10313. https://doi.org/10.1029/2008JA013915

Chum, J., Hruska, F., Zednik, J., & Lastovicka, J. (2012). Ionospheric disturbances (infrasound waves) over the Czech Republic excited by the 2011 Tohoku earthquake. *Journal of Geophysical Research*, *117*, A08319. https://doi.org/10.1029/2012JA017767

Chum, J., Liu, J. Y., Laštovička, J., Fišer, J., Mošna, Z., Baše, J., & Sun, Y. Y. (2016). Ionospheric signatures of the April 25, 2015 Nepal earthquake and the relative role of compression and advection for Doppler sounding of infrasound in the ionosphere. *Earth, Planets and Space*, *68*, 24. https://doi.org/10.1186/s40623-016-0401-9

Dabas, R. S., Das, R. M., Sharma, K., & Pillai, K. G. M. (2007). Ionospheric pre-cursors observed over low latitudes during some of the recent major earthquakes. *Journal of Atmospheric and Solar-Terrestrial Physics*, *69*(15), 1813–1824.

DasGupta, A., Das, A., Hui, D., Bandyopadhyay, K. K., & Sivaraman, M. R. (2006). Ionospheric perturbations observed by the GPS following the December 26th, 2004 Sumatra-Andaman earthquake. *Earth, Planets and Space*, *58*(2), 167–172.

Davies, K., & Baker, D. (1965). Ionospheric effects observed around the time of the Alaskan earthquake of March 28, 1964. *Journal of Geophysical Research*, *70*, 1251–1253.

Occhipinti, G., Dorey, P., Farges, T., & Lognonné, P. (2010). Nostradamus: The radar that wanted to be a seismometer. *Geophysical Research Letters*, *37*, L18104. https://doi.org/10.1029/2010GL044009

Forbes, J. M., Palo, S. E., & Zhang, X. (2000). Variability of the ionosphere. *Journal of Atmospheric and Solar - Terrestrial Physics*, *62*, 685–693.

Hegai, V. V., Kim, V. P., & Liu, J. Y. (2006). The ionospheric effect of atmospheric gravity waves excited prior to strong earthquake. *Advances in Space Research*, *37*(4), 653–659.

Hegai, V. V., Legenka, A. D., Kim, V. P., & Georgieva, K. (2011). Wavelike perturbations in the ionospheric F2-layer observed after the M8.1 Samoa earthquake of September 29, 2009. *Advances in Space Research*, *47*, 1979–1982. https://doi.org/10.1016/j.asr.2011.01.011

Heki, K. (2011). Ionospheric electron enhancement preceding the 2011 Tohoku-Oki earthquake. *Geophysical Research Letters*, *38*, L17312. https://doi.org/10.1029/2011GL047908

Heki, K., & Ping, J. (2005). Directivity and apparent velocity of the coseismic traveling ionospheric disturbances observed with a dense GPS network, Earth Planet. *Sc. Lett.*, *236*, 845–855.

Joshi, L. M., Sripathi, S., Kumar, M. R., & Kherani, E. A. (2017). Simulating the dependence of seismo-ionospheric coupling on the magnetic field inclination Annales Geophysicae. https://doi.org/10.5194/angeo-36-25-018

Kawase, H., & Aki, K. (1989). A study on the response of a soft basin for incident *S, P*, and Rayleigh waves with special reference to the long duration observed in Mexico City. *Bull. Seism. Soc. Am.*, *79*(5), 1361–1382.

Kherani, E. A., Lognonné, P., Kamath, N., Crespon, F., & Garcia, R. (2009). Response of the ionosphere to the seismic triggered acoustic waves: electron density and electromagnetic fluctuations. *Geophysical Journal International*, *176*, 1–13. https://doi.org/10.1111/j.1365-246X.2008.03818.x

Komjathy, A., Yang, Y. M., Meng, X., Verkhoglyadova, O., Mannucci, A. J., & Langley, R. B. (2016). Review and perspectives: Understanding natural-hazards-generated ionospheric perturbations using GPS measurements and coupled modeling. *Radio Science*, *51*, 951–961. https://doi.org/10.1002/2015RS005910

Liu, J. Y., & Sun, Y. Y. (2011). Seismo-traveling ionospheric disturbances of ionograms observed during the 2011 Mw9.0 Tohoku Earthquake. *Earth, Planets and Space*, *63*, 897–902.

Liu, J. Y., Tsai, Y. B., Chen, S. W., Lee, C. P., Chen, Y. C., Yen, H. Y., et al. (2006). Giant ionospheric disturbances excited by the M9.3 Sumatra earthquake of 26 December 2004. *Geophysical Research Letters*, *33*, L02103. https://doi.org/10.1029/2005GL023963

Ma, G., & Maruyama, T. (2003). Derivation of TEC and estimation of instrumental biases from GEONET in Japan. *Annales de Geophysique*, *21*, 2083–2093.

Maruyama, T., Tsugawa, T., Kato, H., Ishii, M., & Nishioka, M. (2012). Rayleigh wave signature in ionograms induced by strong earthquakes. *Journal of Geophysical Research*, *117*, A08306. https://doi.org/10.1029/2012JA017952

Maruyama, T., Tsugawa, T., Kato, H., Saito, A., Otsuka, Y., & Nishioka, M. (2011). Ionospheric multiple stratifications and irregularities induced by the 2011 off the Pacific coast of Tohoku Earthquake. *Earth, Planets and Space*, *63*, 869–873. https://doi.org/10.5047/eps.2011.06.008

Maruyama, T., Shinagawa, H., Yusupov, K., & Akchurin, A. (2017). Sensitivity of ionosonde detection of atmospheric disturbances induced by seismic Rayleigh waves at different latitudes. *Earth, Planets and Space*, *69*, 20.

Maurya, A. K., Venkatesham, K., Tiwari, P., Vijaykumar, K., Singh, R., Singh, A. K., & Ramesh, D. S. (2016). The 25 April 2015 Nepal Earthquake: Investigation of precursor in VLF subionospheric signal, *Journal of Geophysical Research: Space Physics*, *121*, 10,403–10,416. https://doi.org/10.1002/2016JA022721

Najita, K., & Yuen, P. C. (1979). Long-period oceanic rayleigh wave group velocity dispersion curve from HF Doppler sounding of the ionosphere. *Journal of Geophysical Research*, *84*(A4), 1253–1260. https://doi.org/10.1029/JA084iA04p01253

Ogawa, T., Nishitani, N., Tsugawa, T., & Shiokawa, K. (2012). Giant ionospheric disturbances observed with the SuperDARN Hokkaido HF radar and GPS network after the 2011 Tohoku earthquake. *Earth, Planets and Space*, *64*(12), 25. https://doi.org/10.1016/j.asr.2011.01.011

Pulinets, S., & Boyarchuk, K. (2004). Ionospheric Precursors of Earthquakes. Spring

Reddy, C. D., & Seemala, G. K. (2015). Two-mode ionospheric response and Rayleigh wave group velocity distribution reckoned from GPS measurement following Mw 7.8 Nepal earthquake on 25 April 2015. *Journal of Geophysical Research: Space Physics*, *120*, 7049–7059. https://doi.org/10.1002/2015JA021502

Rishbeth, H., & Mendillo, M. (2001). Pattern of F2-Layer Variability. *Journal of Atmospheric and Solar-Terrestrial Physics*, *63*, 1661-1680. https://doi.org/10.1016/S1364-6826(01)00036-0

Rolland, L. M., Lognonné, P., Astafyeva, E., Kherani, E. A., Kobayashi, N., Mann, M., & Munekane, H. (2011). The resonant response of the ionosphere imaged after the 2011 off the Pacific coast of Tohoku earthquake. *Earth, Planets and Space*, *63*, 853–857. https://doi.org/10.5047/eps.2011.06.020

Saito, A., Tsugawa, T., Otsuka, Y., Nishioka, M., Iyemori, T., Matsumura, M., & Choosakul, N. (2011). Acoustic resonance and plasma depletion detected by GPS total electron content observation after the 2011 off the Pacific coast of Tohoku Earthquake. *Earth, Planets and Space*, *63*(7), 64.

Sauli, P., Abry, P., Boška, J., & Duchayne, L. (2006). Wavelet characterization of ionospheric acoustic and gravity waves occurring during the solar eclipse of August 11, 1999. *Journal of Atmospheric and Solar-Terrestrial Physics*, *68*(3-5), 586–598. https://doi.org/10.1016/j.jastp.2005.03.024

Shinagawa, H., Iyemori, T., Saito, S., & Maruyama, T. (2007). A numerical simulation of ionospheric and atmospheric variations associated with the Sumatra earthquake on December 26, 2004. *Earth, Planets and Space*, *59*(9), 1015–1026.

Sripathi, S., Singh, R., Banola, S., Sreekumar, S., Emperumal, K., & Selvaraj, C. (2016). Characteristics of the equatorial plasma drifts as obtained by using Canadian Doppler ionosonde over southern tip of India, J. Geophys. Res. *Space Physics*, *121*, 8103–8120. https://doi.org/10.1002/2016JA023088

Sun, Y.-Y., Liu, J.-Y., Lin, C.-Y., Tsai, H.-F., Chang, L. C., Chen, C.-Y., & Chen, C.-H. (2016). IonosphericF2region perturbed by the 25 April 2015Nepal earthquake. *Journal of Geophysical Research: Space Physics*, *121*(6), 5778–5784. https://doi.org/10.1002/2015JA022280

Sunil, A. S., Bagiya, M. S., Catherine, J., Rolland, L., Sharma, N., Sunil, P. S., & Ramesh, D. S. (2017). Dependence of near field coseismic ionospheric perturbations on surface deformations: A case study based on the April, 25 2015 Gorkha, Nepal earthquake. *Advances in Space Research*, *59*(5), 1200–1208. https://doi.org/10.1016/j.asr.2016.11.041

Torrence, C., & Webster, P. J. (1999). Interdecadal Changes in the ENSO–Monsoon System. *Bulletin of the American Meteorological Society*, *12*, 2679–2690.

Tulasi Ram, S., Sunil, P. S., Ravi Kumar, M., Su, S.-Y., Tsai, L. C., & Liu, C. H. (2017). Coseismic traveling ionospheric disturbances during theMw7.8 Gorkha,Nepal, Earthquake on 25 April 2015from ground and space borne observations. *Journal of Geophysical Research: Space Physics*, *122*, 10,669–10,685. https://doi.org/10.1002/2017JA023860

Yuen, P. C., Weaver, P. F., Suzuki, R. K., & Furumoto, A. S. (1969). Continuous, traveling coupling between seismic waves and the ionosphere evident in May 1968 Japan earthquake data. *Journal of Geophysical Research*, *74*(9), 2256–2264.